CHEMICAL ENGINEERING TRANSACTIONS
VOL. 86, 2021
A publication of AIDIC
The Italian Association of Chemical Engineering
Online at www.cetjournal.it
Guest Editors: Sauro Pierucci, Jiří Jaromír Klemeš

ISBN 978-88-95608-84-6; **ISSN** 2283-9216

Design of an optimal intensified configuration coupling reaction, heat transfer and membrane separation for the direct synthesis of DME from CO_2 and renewable H_2

Chakib R. Behloul[a,*], Jean-Marc Commenge[a], Christophe Castel[a]

[a] Laboratoire Réactions et Génie des Procédés, UMR 7274, Université de Lorraine, CNRS, 1 rue Grandville, F-54000 Nancy, France
chakib-rafik.behloul@univ-lorraine.fr

The challenges of sustainability require to reduce the use of fossil fuels as raw materials and sources of energy, and require the development of techniques allowing the conversion of CO_2 to high added value products. The process intensification has led to the design of innovative configurations and to the development of multifunctional reactors. The integration of multiple functions within a process of DME direct synthesis is studied and the impact of coupled phenomena (reaction, heat exchange and separation) on the reactor performances of the DME direct synthesis is quantified. The effect of the parameters influencing the membrane reactor performance is analysed and presented in this work. The simulation results show that the conventional reactor performance can be improved by the proper coupling of equipment.

1. Introduction

The context of energy transition brings all chemical industries to question and challenge a number of their processes and design habits. The process intensification is evolving in both the research and industrial worlds (Henry et al., 2019). Carbon dioxide CO_2 is released into the atmosphere mainly from power plants, vehicles and other emitters (Catizzone et al., 2017): due to the progressive accumulation of CO_2 in the atmosphere and the environmental taxes on these emissions, the development of techniques to convert CO_2 into useful chemicals is recommended while, at the same time, creating economic wealth. In this context, the DME synthesis, which can have the role of a fuel substitute, and as a raw material for the petrochemical sector has open the way to the valorization of CO_2 by the CO_2 hydrogenation reaction (Centi and Perathoner, 2009). The CO_2 hydrogenation will be even more valuable and advantageous by using a renewable hydrogen (Mignard et al., 2003). Renewable hydrogen may be obtained by water electrolysis technology: excess decarbonated electricity feeds an electrolyzer to generate hydrogen.
The DME synthesis is exothermic, balanced and of industrial interest (Arcoumanis et al., 2008). The DME can be obtained by two different methods, namely, the direct and the indirect methods. For economic reasons (single reactor, removal of a methanol purification and separation system) and thermodynamic reasons (overcoming the thermodynamic limitation for methanol synthesis), the direct synthesis process is preferred, and will be considered as a case study in the present work (Asthana et al., 2017). The direct synthesis requires a single reactor filled with a bifunctional or hybrid catalyst (Cu-ZnO-Al_2O_3/ γ-Al_2O_3, HZSM-5): methanol synthesis and dehydration are performed in the same equipment from synthesis gas. Coupling to both a selective membrane for in situ water removal and to a heat exchange to remove the heat generated by reactions is discussed in this paper.

2. Stoichiometry and kinetic

DME synthesis involves a series of balanced exothermic reactions presented as follows (Nie et al., 2005):

$$CO_2 + 3H_2 \rightleftarrows CH_3OH + H_2O\ ;\ \Delta H_{298K} = -49.5\ kJ/mol \quad (1)$$

$$CO + 2H_2 \rightleftarrows CH_3OH\ ;\ \Delta H_{298K} = -90.7\ kJ/mol \quad (2)$$

$$2CH_3OH \rightleftarrows DME + H_2O\ ;\ \Delta H_{298K} = -23.5\ kJ/mol \quad (3)$$

Reaction rates are written as follows (Nie et al., 2005):

$$r_1 = \frac{k_1\, f_{CO_2} f_{H_2}^3 \left(1 - \frac{f_{CH_3OH} f_{H_2O}}{K_{eq_1} f_{CO_2} f_{H_2}^3}\right)}{\left(1 + K_{CO_2} f_{CO_2} + K_{CO} f_{CO} + K_{H_2} f_{H_2}\right)^4} \quad (4)$$

$$r_2 = \frac{k_2\, f_{CO} f_{H_2}^2 \left(1 - \frac{f_{CH_3OH}}{K_{eq_2} f_{CO} f_{H_2}^2}\right)}{\left(1 + K_{CO_2} f_{CO_2} + K_{CO} f_{CO} + K_{H_2} f_{H_2}\right)^3} \quad (5)$$

$$r_3 = \frac{k_3\, f_{CH_3OH} \left(1 - \frac{f_{DME} f_{H_2O}}{K_{eq_3} f_{CH_3OH}^2}\right)}{\left(1 + \sqrt{K_{CH_3OH} f_{CH_3OH}}\right)^2} \quad (6)$$

The kinetic parameters are listed in **Table 1**.

Table 1: Kinetic parameters (Nie et al., 2005)

Parameter	Expression	Unit
k_1	$1.4053 * 10^{-17} \exp(-67515/RT)$	mol/kg s Pa^4
k_2	$2.05 * 10^{-12} \exp(-54307/RT)$	mol/kg s Pa^3
k_3	$2.95 * 10^{-3} \exp(-43473/RT)$	mol/kg s Pa
K_{CO}	$3.934 * 10^{-11} \exp(37373/RT)$	Pa^{-1}
K_{CO_2}	$1.858 * 10^{-11} \exp(53795/RT)$	Pa^{-1}
K_{H_2}	$0.6716 * 10^{-5} \exp(-6476/RT)$	Pa^{-1}
K_{CH_3OH}	$3.48 * 10^{-11} \exp(54689/RT)$	Pa^{-1}

In the case of a CO_2-rich feed, the DME synthesis is inhibited, and thus, the reactor performance is reduced (Ereña et al., 2005). Such a negative effect is mainly related to the progressive water accumulation that inhibits the methanol dehydration kinetics (reaction (3)) and the CO_2 hydrogenation (reaction (1)). Taking into account these inhibition effects and thermodynamic limitations, as well as the requirements for higher efficiency and conversion, the process intensification is envisaged. The integration of multiple functions within a process is a potential source of economic and energy gains, especially when the process can be intensified through reasoned coupling to separation equipment. In order to intensify the DME direct synthesis process, coupling to a selective membrane separation for in situ water removal is a promising way forward.
In this work, an analysis of the performance of a membrane reactor configuration (MR) will be assessed, then compared to a conventional reactor configuration (CR).

3. Mathematical modeling

The membrane reactor (MR) considered is a tubular fixed bed reactor equipped with a membrane (**Figure 1**).

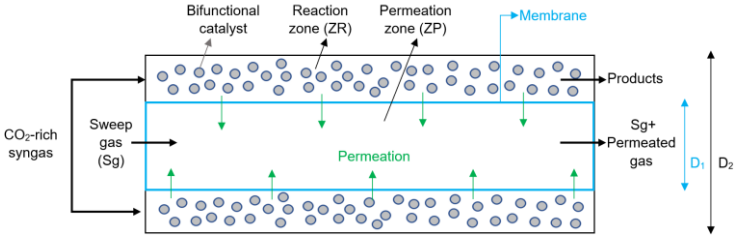

Figure 1: Schematic of proposed configuration (MR).

The reactor consists of two co-axial tubes (Farsi and Jahanmiri, 2011). It is divided into two zones: reaction zone (ZR) and permeation zone (ZP). The inner tube (D_1) in which the inert sweep gas flows in co-current with respect to the feed, is the water perm-selective membrane surrounded by the reaction zone. The annular space between the outer tube (D_2 = 3 cm) and the inner tube (D_1 = 2 cm) is the reaction zone where the catalytic particles are packed.
The membrane used must be adequate with the operating conditions for DME synthesis. It has been shown that zeolite membranes are the most suitable for temperatures above 200°C: the water permeance $\mathcal{P}_{H_2O}$ varies in the range 10^{-7} and 10^{-6} mol/ (m^2 s Pa) for a H_2O/H_2 selectivity higher than 10 at T = 250 °C (Rohde et al., 2008).
The assumptions considered are as follows: (i) ideal behavior is assumed for the gas mixture, (ii) 1D plug flow model, simulated at steady state, (iii) isothermal conditions for both reaction and permeate zones $(dT/dz = 0)$, (iv) reactions occur on catalyst surface: no fluid-to-particle heat and mass transfer resistances.
In order to assess the molar fluxes variation of species within the ZR and ZP as a function of the axial position z of the reactor, it is necessary to solve the differential equations given by equations (7) and (8).

$$\frac{dF_i^{ZR}}{dz} = \frac{\pi}{4}(D_2^2 - D_1^2)\,\rho_{app}\sum_{j=1}^{m}\vartheta_{i,j}\,r_j - \pi D_1\varphi_i \qquad (1 \le i \le n) \tag{7}$$

$$\frac{dF_i^{ZP}}{dz} = \pi D_1\varphi_i \qquad (1 \le i \le n) \tag{8}$$

Where j denotes the reaction index and i the species index $(CO_2, H_2, CO, H_2O, CH_3OH, DME, inert)$. In these equations, m denotes the number of reactions, n the number of species present in the reaction medium, F_i the molar flux of species i, D_1 and D_2 the internal and external tube diameters, respectively, ρ_{app} the density of the catalyst bed, r_j the rate of reaction j, $\vartheta_{i,j}$ the stoichiometric coefficient of species i in reaction j, and φ_i the trans-membrane molar flux for species i computed by equation (9). Only the water and hydrogen permeance ($\mathcal{P}_i$) will be considered in this case: $(S_{H_2O/H_2} > 10\,, S_{H_2O/i} = \infty)$.

$$\varphi_i = \mathcal{P}_i\left(P_i^{ZR} - P_i^{ZP}\right) \tag{9}$$

The pressure drop in the catalyst bed (spherical particles) is estimated with the Ergun equation (equation (10)).

$$\frac{dP}{dz} = -\left(150\frac{(1-\varepsilon_{bed})^2}{\varepsilon_{bed}^3}\frac{\mu\,u_m}{d_p^2} + 1.75\frac{1-\varepsilon_{bed}}{\varepsilon_{bed}^3}\frac{\rho_f\,u_m^2}{d_p}\right) \tag{10}$$

Where ε_{bed} represents the external porosity of the catalytic bed, u_m the superficial velocity of the fluid in the fixed bed, d_p the particles diameter, μ the dynamic viscosity of the fluid and ρ_f its density. The "ode15s" solver, adapted to stiff systems, has been chosen as a numerical method for solving the differential balance equations implemented in MATLAB R2019.

4. Results and discussion

Figure 2 presents both the evolution of water partial pressure in the CR and in the MR within the two zones for two different molar sweep gas flow rates.

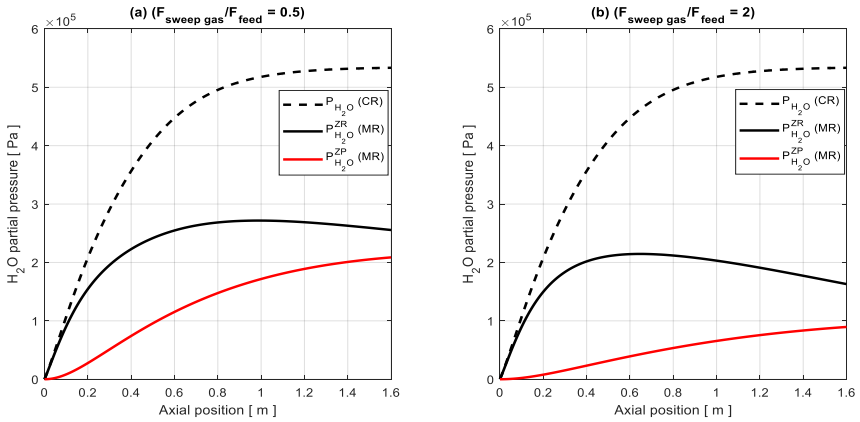

Figure 2: Influence of the $F_{sweep\ gas}/F_{feed}$ ratio ((a): 0.5 and (b): 2) on the water partial pressure in both zones (ZP and ZR). (CR: discontinuous lines, MR: continuous lines) $(T_{in} = 260\,°C, P_{in}^{ZR} = 5\,MPa,\ GHSV = 4500\,h^{-1}, H_2/CO_2 = 3, CO_2/CO = 8, P_{in}^{ZP}/P_{in}^{ZR} = 0.25\,)$.

In the CR, the partial pressure profile of water increases and tends towards an equilibrium plateau at the reactor outlet. **Figure 2** shows that the partial pressure of water profiles in the ZR of the MR and in the CR are very close in the first part of the reactor (feed side): no intensification is brought by the membrane in this area. This can be explained by the rapid production of water compared to its removal rate through the membrane, reason why the water partial pressure profiles within the MR first passes through a maximum and then gradually decreases. At $F_{sweep\ gas}/F_{feed} = 0.5$, the sweep gas is more quickly saturated with water than at a ratio $F_{sweep\ gas}/F_{feed} = 2$, inducing a higher water partial pressure in the ZR. At $F_{sweep\ gas}/F_{feed} = 2$, a higher water partial pressure difference between the two zones leads to a high driving force for the water permeance through the membrane. It is worth noting that the sweep gas flow rate setting influences the MR performance.
In order to quantify the impact of the $F_{sweep\ gas}/F_{feed}$ factor on the MR performance, another factor which expresses the ratio between the inlet total pressures of the two zones P_{in}^{ZP}/P_{in}^{ZR} will be considered, and the results are presented in **Figure 3**. The MR performance are assessed in terms of CO_X (CO_2+CO) conversion, of CO_2 conversion, and of yield and selectivity of DME defined in **Table 2**.

Table 2: Operating conditions and expressions allowing to quantify the MR performance

Parameter	Value	Parameter	Expression
$F_{sweep\ gas}/F_{feed}$	$[0.5-5]$	X_{CO_x}	$1-\left(F_{CO_2}+F_{CO}\right)_{out}/\left(F_{CO_2}+F_{CO}\right)_{in}$
P_{in}^{ZP}/P_{in}^{ZR}	$[0.01-0.6]$	y_{DME}	$2F_{DME_{out}}/\left(F_{CO_2}+F_{CO}\right)_{in}$
$P_{in}^{ZR}\ (MPa)$	5	X_{CO_2}	$1-F_{CO_2\,out}/F_{CO_2\,in}$
GHSV (h^{-1})	4500	S_{DME}	$2\,F_{DME_{out}}/\left(2F_{DME}+F_{CH_3OH}\right)_{out}$
$P_{H_2O}\ (mol/(m^2\ s\ Pa))$	$4*10^{-7}$		

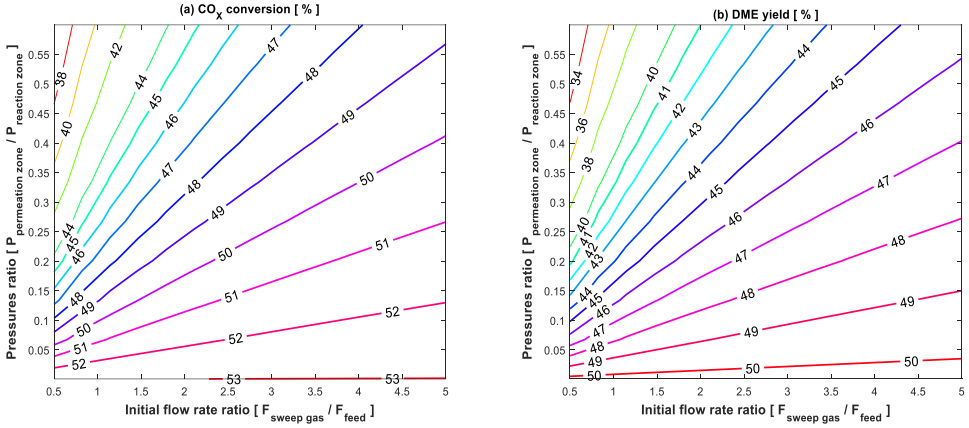

Figure 3: Effect of the $F_{sweep\ gas}/F_{feed}$ and P_{in}^{ZP}/P_{in}^{ZR} ratios on the MR performance at 260 °C.

It should be noted that the same trends are obtained for the effect of these ratios on the DME selectivity and the CO_2 conversion. **Figure 3** shows that the decrease of the P_{in}^{ZP}/P_{in}^{ZR} ratio creates a higher transmembrane driving force (high pressure difference between the two zones). Similarly, increasing the sweep gas flow rate (increasing the $F_{sweep\ gas}/F_{feed}$ ratio) has a positive effect on the MR performance more particularly when $P_{in}^{ZP}/P_{in}^{ZR} \geq 0.2$. A high appropriate sweep gas flow rate keeps the water partial pressure in the permeation zone as low as possible, therefore, the transmembrane flux φ_i through the membrane is higher. It is worth mentioning that the use of a high sweep gas flow rate at low P_{in}^{ZP}/P_{in}^{ZR} ratio, or the choice of vacuum conditions ($P_{in}^{ZP} \approx 0$) with a high sweep gas flow rate has no significant impact on the MR performance under these conditions. **Figure 3** indicates that there is a trade-off between these two factors in order to maintain a high transmembrane driving force without consuming excessive energy to maintain a significant pressure difference between the two zones.
According to the cartographic representations in **Figure 3**, a $P_{in}^{ZP}/P_{in}^{ZR} = 0.1$ and a $F_{sweep\ gas}/F_{feed} = 2.5$ ratios are chosen to allow the comparison between the performance of MR proposed and the CR presented in the **Figure 4** and the **Table 3**.
In the CR, the thermodynamic equilibrium is almost reached at the reactor outlet as shown by the dashed line profiles in **Figure 4**. The intensification by coupling with membrane separation for water in situ removal from the reaction zone clearly increases the reactor performance as shown in **Figure 4** and reported in **Table 3**.

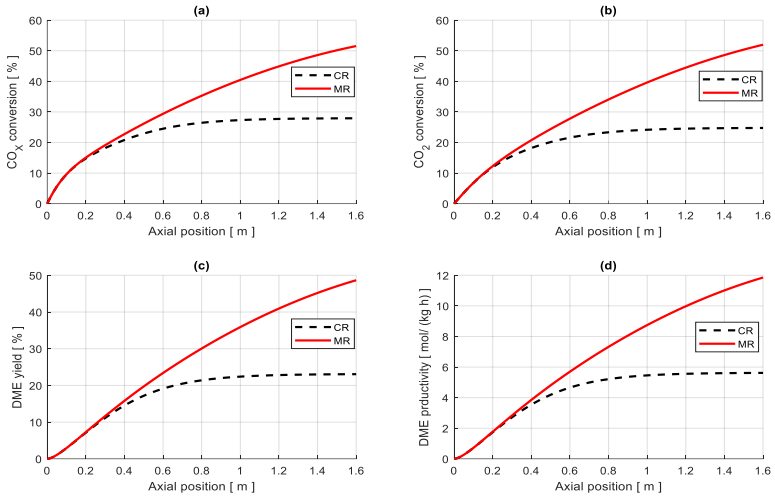

Figure 4: Comparison of simulation results obtained in the CR and MR at T_{in} = 260 °C, GHSV = 4500 h^{-1}, H_2/CO_2 = 3, CO_2/CO = 8, $P_{in}^{ZR} = 5\ MPa$, $P_{in}^{ZP}/P_{in}^{ZR} = 0.1$ and $F_{sweep\ gas}/F_{feed} = 2.5$.

Table 3: Comparison between the performance of MR proposed and the CR

Parameter	CR	MR
CO_X conversion (%)	27.93	51.54
CO_2 conversion (%)	24.76	51.97
DME yield (%)	23.06	48.65
DME productivity (mol/ (kg h))	5.62	11.85

In order to study the effect of the coupling between reaction, heat exchange and membrane separation on the final conversion and on the thermodynamic equilibrium, the heat balance is added to the set of equations mentioned above (equations (7)-(10)). The heat balance expressed by equation (11) is established by assuming that the membrane has no resistance to heat transfer (temperature in ZP is assumed the same as in ZR).

$$\frac{dT}{dz} = \frac{\frac{\pi}{4}(D_2^2 - D_1^2)\rho_{app} \sum_{j=1}^{m} (-\Delta H_j)\, r_j - \pi D_2 U (T - T_f)}{\sum_{i=1}^{n_t} F_i Cp_i} \tag{11}$$

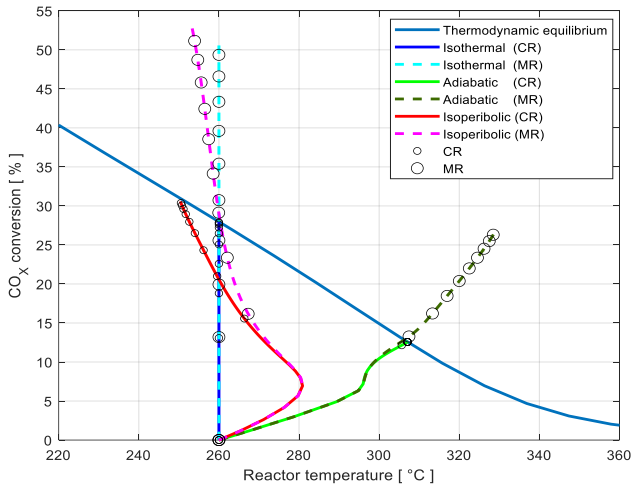

Figure 5: Impact of the coupling of reaction, heat exchange and separation on the achieved equilibrium (T_{in} = 260 °C, T_f = 250 °C, GHSV = 4500 h^{-1}, H_2/CO_2 = 3, CO_2/CO = 8, $P_{in}^{ZR} = 5\ MPa$, $P_{in}^{ZP}/P_{in}^{ZR} = 0.1$, $F_{sweep\ gas}/F_{feed} = 2.5$).

Where T is the local temperature, ΔH_j the enthalpy of reaction j at temperature T, U the overall heat-transfer coefficient, T_f the temperature of the coolant and Cp_i the heat capacity at constant pressure of species i.

Figure 5 shows the axial evolutions (trajectories in the plane (Temperature; Conversion)) in isothermal, adiabatic and isoperibolic modes. The distance between successive circles along the trajectories represents one tenth of the reactor length. Coupling to a selective hydrophilic membrane overcomes the thermodynamic barrier, and shifts the output conversion in the enhancement direction. This being said, the selective removal of water shifts the equilibrium in the direction of methanol production (reagents conversion sense), which is instantaneously transformed into DME. In the case of an adiabatic membrane reactor, the temperature of the mixture exceeds 300°C, which could lead to membrane damage. Therefore, an adiabatic membrane reactor configuration is not preferable to the other two cases (isothermal and isoperibolic). For an isoperibolic reactor, even with a membrane coupling, the two profiles have the same trajectory in the first tenth of the reactor about (distance between two successive circles). This last point shows that the water removal rate through the membrane is lower than the water production and heat generation rates in the reaction zone. It can be said that under these operating conditions, the configuration proposed (MR) is controlled by the water removal rate. In the same way, the adiabatic trajectory starts with the same slope as the isoperibolic trajectory, meaning that the heat generation rate is faster than that which can be transferred to the heat transfer fluid.

5. Conclusions

The intensification of the DME direct synthesis from CO_2 and H_2 is studied in order to improve the process efficiency. The performance of the proposed configuration is compared to the CR at 260 °C and 5 MPa. The in situ water removal overcomes thermodynamic limitations while increasing CO_2 conversion and desired product yield (DME). A trade-off between $F_{sweep\ gas}/F_{feed}$ and P_{in}^{ZP}/P_{in}^{ZR} ratios should be chosen to ensure optimum trans-membrane driving force. The MR configuration can be limited by the water removal rate.

Acknowledgments

The authors acknowledge the French MESRI for their financial support of research works.

References

Arcoumanis, C., Bae, C., Crookes, R., Kinoshita, E., 2008. The potential of di-methyl ether (DME) as an alternative fuel for compression-ignition engines: A review. Fuel 87, 1014–1030. https://doi.org/10.1016/j.fuel.2007.06.007

Asthana, S., Samanta, C., Voolapalli, R.K., Saha, B., 2017. Direct conversion of syngas to DME: synthesis of new Cu-based hybrid catalysts using Fehling's solution, elimination of the calcination step. J. Mater. Chem. A 5, 2649–2663. https://doi.org/10.1039/C6TA09038A

Catizzone, E., Bonura, G., Migliori, M., Frusteri, F., Giordano, G., 2017. CO_2 Recycling to Dimethyl Ether: State-of-the-Art and Perspectives. Molecules 23, 31. https://doi.org/10.3390/molecules23010031

Centi, G., Perathoner, S., 2009. Opportunities and prospects in the chemical recycling of carbon dioxide to fuels. Catalysis Today 148, 191–205. https://doi.org/10.1016/j.cattod.2009.07.075

Ereña, J., Garoña, R., Arandes, J.M., Aguayo, A.T., Bilbao, J., 2005. Direct Synthesis of Dimethyl Ether From (H_2+CO) and (H_2+CO_2) Feeds. Effect of Feed Composition. International Journal of Chemical Reactor Engineering 3 (1), A44. https://doi.org/10.2202/1542-6580.1295

Farsi, M., Jahanmiri, A., 2011. Mathematical simulation and optimization of methanol dehydration and cyclohexane dehydrogenation in a thermally coupled dual-membrane reactor. International Journal of Hydrogen Energy 36, 14416–14427. https://doi.org/10.1016/j.ijhydene.2011.08.019

Henry, G., Pere-Gigante, A., Siewert, J., Valentin, S., Wagner, M., Commenge, J.-M., 2019. Design and Experimental Study of a Milli-channel Vaporizer. Chemical Engineering Transactions 74, 1327–1332. https://doi.org/10.3303/CET1974222

Mignard, D., Sahibzada, M., Duthie, J.M., Whittington, H.W., 2003. Methanol synthesis from flue-gas CO_2 and renewable electricity: a feasibility study. International Journal of Hydrogen Energy 28, 455–464. https://doi.org/10.1016/S0360-3199 (02)00082-4

Nie, Z., Liu, H., Liu, D., Ying, W., Fang, D., 2005. Intrinsic Kinetics of Dimethyl Ether Synthesis from Syngas. Journal of Natural Gas Chemistry 14 (1), 7.

Rohde, M.P., Schaub, G., Khajavi, S., Jansen, J.C., Kapteijn, F., 2008. Fischer–Tropsch synthesis with in situ H_2O removal – Directions of membrane development. Microporous and Mesoporous Materials, 4th International Zeolite Membrane Meeting 115, 123–136. https://doi.org/10.1016/j.micromeso.2007.10.052